Thermal perfomance of additively manufactured heat pipes

Borja Cobo-Lopez[a,*], J. Rodríguez-Rodríguez[b], D. Orgaz[a], C. Sobrino[b]

[a] *Madrid Space S.L., Av. Gregorio Peces Barba, 1, 28919 Leganés, Madrid, Spain*
[b] *Universidad Carlos III de Madrid, Thermal and Fluid Engineering Department, Avda. de la Universidad 30, 28911 Leganés, Madrid, Spain*

Abstract

This work studies experimentally the performance of an additively manufactured heat pipe with a triangular cross-section and grooved wick that uses acetone as the heat transfer fluid. The temperature time evolution at different axial positions of the heat pipe was measured for different heat transfer rates and fluid filling inventories. The experimental data analysis includes calculating heat losses and estimating the steady-state temperature, which has been shown to be critical for determining the thermal resistance and time constant accurately. We also propose a methodology to estimate the response time of the heat pipe to sudden changes in the thermal power demand. The presented prototype is able to evacuate up to 17 W in horizontal position with a thermal resistance lower than 1 $\mathrm{K\,W^{-1}}$.

Keywords: Heat pipes, 3D-printing

1. Introduction

Heat pipes are devices that transport heat between two spatial locations over a small temperature gradient. They find applications in very diverse

*Corresponding author
Email address: b.cobo@madridspace.eu (Borja Cobo-Lopez)

fields like nuclear engineering, geothermal heat harvesting or aerospace [1]. The case of aerospace applications is particularly challenging, as electronic components are increasing their performances very fast, which translates into tighter heat dissipation demands that require technological leaps in heat pipe technology [2]. One of the most promising technologies to enable this leap is additive manufacturing. Additive manufacturing is able to provide lightweight structures with optimized geometries while exhibiting good mechanical and thermal properties. In recent times, 3D-printed heat pipes have been tested in different contexts [3, 4, 5, 6]. We summarize next some works of special relevance for our study.

An aluminum 3D-printed heat pipe with microgrooves and working with acetone was tested and applied to the thermal management of a LED [4]. Other authors have also tested 3D-printed heat pipes in a CubeSat Thruster, requiring a heat dissipation of 15 W [7]. Porous structures and acetone as the working fluid were chosen in this study. The experiments showed good performance in thermosiphon and horizontal orientation. Nevertheless, it starts to deteriorate at inclinations of -2° (with respect to the horizontal plane), leading to the drying out of the wick at the evaporator. Esarte and co-workers measured methanol imbibition in stainless-steel porous wicks manufactured by selective laser melting, a 3D printing technology [3]. This study showed higher permeability values, and thus faster imbibition, than in a conventional copper wick manufactured by powder sintering. However, the imbibition speed was lower than that of a stainless-steel mesh. Jafari *et al.* [8] performed experiments to study the thermal performance of an additively manufactured stainless steel heat pipe working with water, focusing also on the optimal inventory (mass of working fluid) that a non-conventional, 3D-printed wick design needs. They conclude that the optimum filling ratio

was 110% of the amount of fluid required to saturate the wick. Alternatively, Chang *et al.* [4] defined the filling ratio as the proportion between the volume of loaded working fluid and the inner space of the heat pipe, finding that a filling ratio of 10% gave the best heat transfer performance with the lowest thermal resistance. The enhanced performance compared to conventional wick structures was attributed to an increase in the evaporating meniscus density at the liquid-vapor interface due to the presence of sintered powder features. Park and collaborators [5] recently presented a heat pipe with improved capillary transport and permeability, fabricated using 3D printing technology, that includes a hybrid screen-groove wick in the evaporator section and a homogeneous groove wick in the adiabatic and condenser sections. They attribute the good wicking properties of their design to the additional roughness that the manufacturing technique endows the wick surface. Finally, Yun and co-workers [6] tested an aluminum heat pipe manufactured with selective laser melting that uses acetone as working fluid. They obtain similar conclusions regarding the improved wicking capabilities, as compared to other conventional manufacturing techniques. They also present a mathematical model of the heat pipe performances which describe well their experimental measurements when the inventory is 100% of the wick volume. Interestingly, for an inventory of 150%, the performances seem to be better than expected.

In view of the works just described, laser powder bed fusion emerges as the most popular technique for the additive manufacturing of metallic heat pipe wicks. Given the novelty of the application of this technique to the manufacturing of heat pipes, further research, including the design of innovative geometries that can reduce the manufacturing cost, is needed. Moreover, the issue of the optimal inventory seems to be quite open. Another

topic that is not sufficiently studied in these innovative designs is that of the transient times the heat pipe takes to reach a steady state upon a sudden change in the thermal boundary conditions. With these ideas in mind, we present hear a new heat pipe design, manufactured with laser melting technology. We put emphasis on understanding the effect of the inventory on the heat pipe performances, characterized by the effective thermal resistance and by the transient time taken to reach steady operation after a sudden change in the evaporator temperature. To be able to carry out systematic studies on the effect of the fluid inventory, we present the design of an improved heat pipe test-bench that allows to try different inventories in a same heat pipe instance without having to unmount it. The design of the facility includes simple algorithms to estimate heat losses to the ambient and to determine the final temperature reached after long transient times without the need to wait until a steady state is fully reached. The proposed methodology offers the possibility to speed up the testing of novel heat pipe designs and their sensitivity to different operating conditions, including their inclination or the fluid inventory.

2. Materials and Methods

2.1. Overall description of the facility and the filling procedure

A test bench was built (Fig. 2) to study the thermal performance of an additively manufactured heat pipe at different inclinations, fluid inventories and thermal demands. The tested prototype is 140 mm long with an external quasi-triangular shape made of aluminum. The base of the triangle is 14.5 mm wide. The inner cross-section is 60 mm^2 and the wick is made of rectangular grooves distributed along the three sides of the pipe (figure 1).

The pipe's triangular design allows for additive production of the pipe in a horizontal position without the need for support structures, simplifying process planning and reducing waste material. In order to assess the heat pipe's performance, experiments were conducted to measure its thermal resistance for different working conditions.

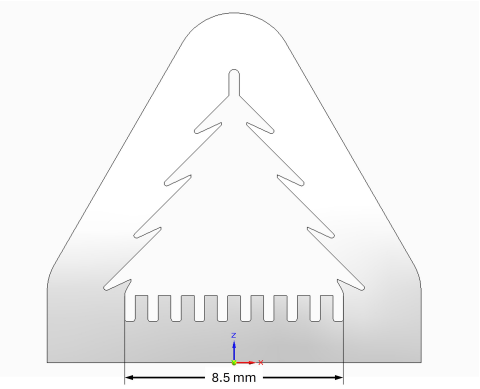

Figure 1: CAD view of the prototype internal cross-section

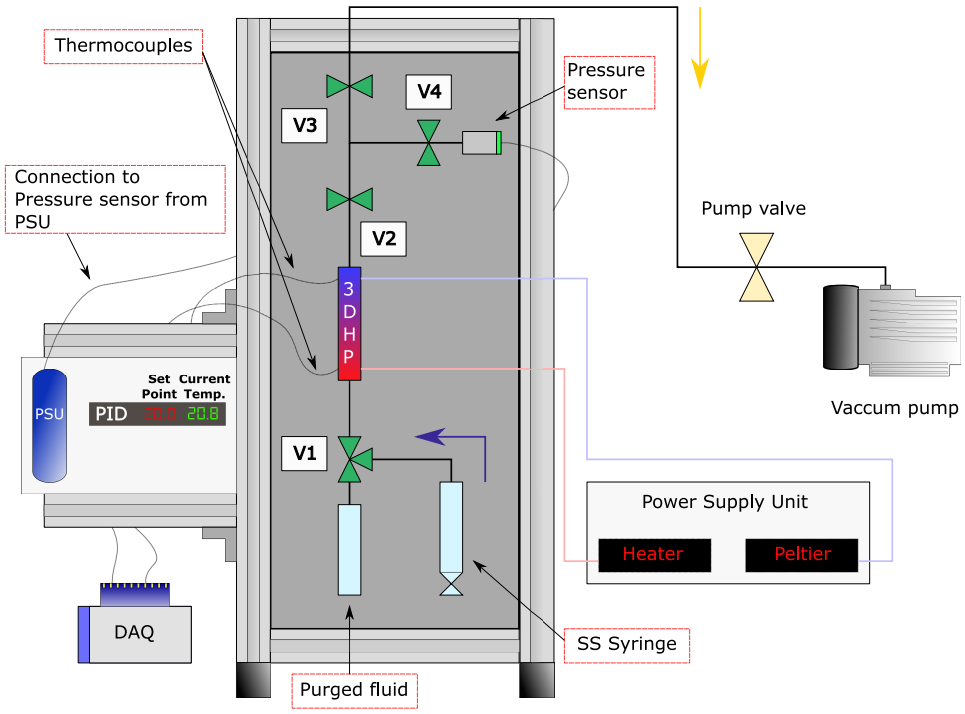

Figure 2: Experimental set-up

The test bench shown in Fig. 2 was built for vacuuming the heat pipe, filling it up and measuring its thermal resistance in an efficient way in a variety of conditions. The vacuum line (shown as a yellow arrow in Fig. 2) is connected from a stainless-steel valve (V3) to the vacuum pump, which isolates the pump from the rest of the circuit. The vacuum pump is a dry scroll pump (Scrollvac 10 plus) that provides a minimum pressure within the prototype of 0.10 mbar previously to filling it with the working fluid. Downstream V3, the main line forks into two paths. On the one hand, the right line that joins with V4 protects the pressure sensor from chemical attack by the working fluid (Acetone). On the other hand, the bottom line connects with the test prototype through valve V2. The pressure inside the

pipe is measured with a TTR 200 NS MEMS Pirani sensor with a range of $5 \cdot 10^{-5}$ mbar to 1500 mbar. This device is connected to a 24-V power supply unit (PSU).

Before filling the heat pipe with the working fluid, we vacuum the installation. To do this, valves V2, V3 and V4 are opened (while V1 remains closed) prior to starting the vacuum process. To verify that there are no leaks in the circuit, a helium leak detector was used to ensure the tightness of each connection. All connections showed a leak rate under $10^{-9}\,\mathrm{mbar\,l\,s^{-1}}$. In addition to the vacuum pump, the same heater that supplies heat to the heat pipe's evaporator is activated to assist in the removal of condensable gases. Once a minimum pressure of 0.10 mbar is reached within the circuit, V3 and the pump valve are closed. Subsequently, the heat pipe can be filled through the designated pathway, marked by a blue arrow in Fig. 2. The filling process is done using a 20 ml stainless-steel syringe with a 0.5 ml resolution. This syringe is connected to the 3-way stainless steel valve (V1) where one way connects to the heat pipe through a narrow conduit, and the other is used to drain out the excess fluid used to feed and purge air from the filling circuit. To charge the circuit and ensure that the syringe only contains the required amount of fluid, valve V1 first connects the syringe with the line intended for the removal of excess liquid. After that, valve V1 is turned to the position that connects the heat pipe and the syringe. The volume of the internal grooves, the volume of the tube connecting the heat pipe to valve V1, and the dead volume of valve V1 are calculated from prototype 3D models and added together to calculate the geometrical fluid inventory (V_{geom}). Subtracting the volume of the tube connecting the heat pipe to valve V1 and the dead volume of valve V1 to V_{geom} yields the volume that will fill the heat pipe itself. This is referred to as the effective

fluid inventory (V_{eff}). The heat pipe must not be underfilled or overfilled, as underfilling will result in performance degradation and overfilling will result in condenser blockage [9]. In principle, the optimal fluid inventory is the volume required to fill the wick with liquid and the vapor core with gas. The volume required to fill the vapor core may be neglected because it is far greater than the volume needed to fill the wick, owing to the large density ratio between the liquid and its vapour. The initial filling of the feeding circuit with working fluid is essential to minimize the amount of non-condensable gases (air) introduced inside the heat pipe. Because it is unavoidable to introduce some non-condensables during the filling, after the pipe has been filled with the desired fluid inventory, the vacuum circuit is opened (via valve V3) for a few seconds to eliminate its gas content. This procedure is very efficient in eliminating non-condensables while having a moderate impact on the amount of working fluid left inside the heat pipe due to the large ratio between the vapor and liquid density.

2.2. Description of the testing procedure

In our experimental facility, once the filling is completed, the heat pipe is not separated from the feeding circuit. This has the advantage of allowing us to evaluate the performance of the prototype for different fluid inventories in an easy and inexpensive way. However, it brings the disadvantage of worse thermal insulation, as some heat will be lost to conduction through the feeding circuit. Nonetheless, this is not a serious disadvantage, as we can correct the measured heat pipe performances to account for the effect of these losses (see Section 2.4 below).

In the heat pipe, heat is transferred to the evaporator by means of a

cartridge heater embedded in an aluminum block (Fig. 3). The surface area where the heat is applied is equal to 30 mm×14.5 mm. The condenser heat is evacuated through a Peltier cell equipped with a fan-cooled heatsink. The evaporator and condenser are both 30 mm long, and the adiabatic region between them is 80 mm long. The temperature distribution is measured by ten T-type thermocouples distributed along the longitudinal axis and at both external and lateral sides of the evaporator and condenser regions.

The thermocouple placed at the condenser surface is used as input signal of a Omega CN7500 PID controller to set the cold temperature during the experiments. Every thermocouple and the pressure sensor are connected to a NI-cDAQ system, which acquires data with a 10 Hz framerate. The assembly is isolated from the ambient with Teflon, CPE (chlorinated polyethylene elastomer) material, and neoprene foam.

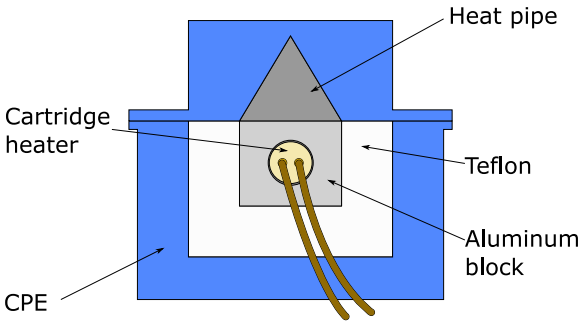

Figure 3: Scheme of cartridge heater embedded in an aluminum block encapsulated with Teflon and CPE.

To evaluate the performance of the heat pipe, the thermal resistance (Fig. 4) was determined as

$$R_{hp} = \frac{T_{p,e} - T_{p,c}}{Q_{hp}} \tag{1}$$

where $T_{p,e}$ is the temperature of the outer surface of the evaporator at the furthest axial position from the condenser, $T_{p,c}$ is the temperature of the outer surface of the condenser at the furthest axial position from the evaporator and Q_{hp} is the heat transfer rate that is effectively applied to the heat pipe.

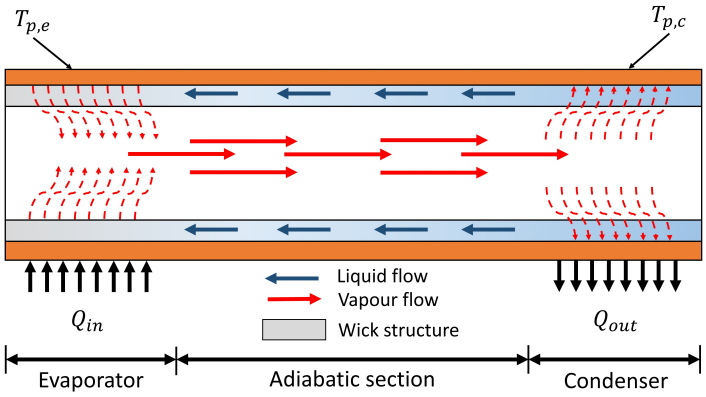

Figure 4: Scheme of the measured thermal resistance.

The resistance was measured for different heat transfer rates in the range of 0 to 20 W. The heat transfer rate is controlled by varying the input voltage to the heater by a power supply unit capable of delivering up to 60 VDC. On the other hand, the PID controller described above, is connected with a solid-state relay to the Peltier cell that refrigerates the condenser. The Peltier is switched off when the temperature decreases below the set point for the outer surface of the condenser, which is set to 20 °C in all experiments reported here.

The heat transfer fluid selected for the heat pipe prototype was acetone.

Heat pipes commonly use acetone, ammonia, ethanol, methanol or methylamine as working fluids. Water cannot be used as heat transfer fluid due to its incompatibility with aluminum, since the hydrogen generated during the experiments causes the degradation of the heat pipe performance [10].

2.3. Steady-state temperature

During the experiments, it was observed that for the highest heat transfer rates, it required a considerable amount of time ($> 1\,\mathrm{h}$) for the temperature of the pipe envelope to reach a steady state. This may lead to very long testing times if we are to be sure that the steady state has been reached. To overcome this difficulty, the measured temperature time evolution were fitted with the following equation to extrapolate the final steady-state temperature:

$$T_{\mathrm{fit}}(t) = T_\infty - (T_\infty - T_0)e^{-\frac{t-t_0}{\tau}} \tag{2}$$

where T_{fit} is the estimated temperature profile, T_∞ is the steady-state temperature reached at each stage, t is the time vector at each stage, τ is the time exponential decay and t_0 and T_0 are the initial time and temperature at the corresponding stage, respectively. Fig. 5 illustrates an example of how Eq. (2) was applied to one of our experimental temperature time evolutions.

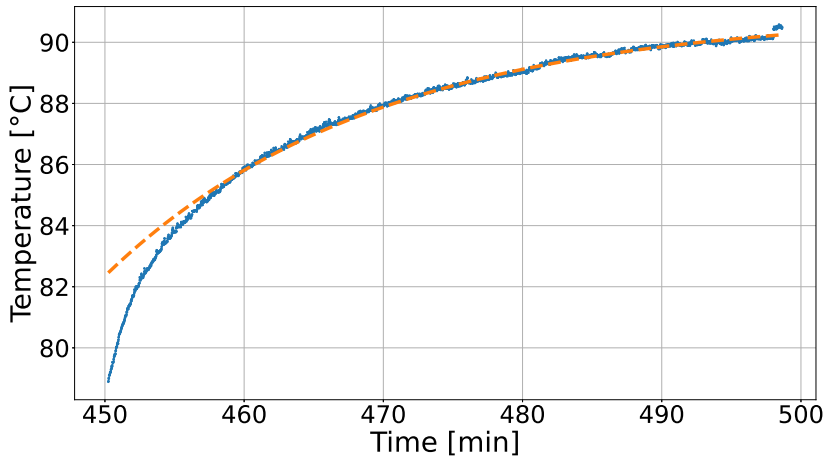

Figure 5: Comparison of the evaporator temperature time evolution (blue line) and the Eq. (2) (dashed orange line) measured in horizontal position and for a $Q_{in} = 21.00\,\mathrm{W}$ and a fluid inventory of 2 ml.

The associated parameters of the temperature time evolution displayed in Fig. 5 are $T_\infty = 90.95$ °C and $\tau = 1164.90$ s.

2.4. Heat loss to the environment

The tested prototype is thermally insulated from the environment, as explained in Section 2; however, the specimen is connected to the vacuum and filling lines by stainless-steel valves, and thus a non-negligible amount of heat supplied by the cartridge heater is not only transferred to the heat pipe but also lost through the connection lines. As a result, we propose the following expression to account for the losses to the environment as well as through the connection lines:

$$Q_{in} = Q_{hp} + Q_{loss} \tag{3}$$

where Q_{in} is heat supplied by the heater, Q_{hp} is the heat transfer rate that actually goes to the prototype and Q_{loss} are heat losses. Eq. (3) is developed as a function of evaporator, condenser, and room temperature. A batch of dry-tests with the pipe empty of fluid were performed at different heat transfer rates (Q_{in}) to estimate the fitting parameters of our model

$$Q_{in} = \frac{T_{p,e} - T_{p,c}}{R_{dry}} + K_{loss} \mid T_{p,e} - T_{amb} \mid^{\alpha_{loss}} \tag{4}$$

where the experimental data are the evaporator temperature $T_{p,e}$, condenser temperature $T_{p,c}$, and the room temperature T_{amb}. The fitting parameters are the heat pipe thermal resistance from dry-tests (R_{dry}) and the losses to the environment and the connection lines (K_{loss} and α_{loss}).

The aforementioned fitting parameters are estimated according to the following steps:

1. We define a cost function representing the sum of the squared error between the experimental values of $T_{p,e}$, $T_{p,c}$, and T_{amb} and the numerical ones computed using Eq. (4):

$$\varepsilon^2(R_{dry}, K_{loss}, \alpha_{loss}) = \sum_{n=1}^{N} \mid Q^2_{\text{num}}(R_{dry}, K_{loss}, \alpha_{loss}) - Q^2_{\text{exp}}(T_{p,e}, T_{p,c}, T_{amb}) \mid \tag{5}$$

   In this expression, $Q_{\text{num}}(R_{dry}, K_{loss}, \alpha_{loss})$ is the numerical solution of the heat transfer rate of Eq. (4), whereas $Q_{\text{exp}}(T_{p,e}, T_{p,c}, T_{amb})$ is an experimental value for the heat transfer rate. The experimental data from tests performed with the empty heat pipe can be found in Supplemental Material.

2. We find the set of parameters $(R_{dry}, K_{loss}, \alpha_{loss})$ that minimizes this cost function for a given experimental curve $Q_{\exp}(T_{p,e}, T_{p,c}, T_{amb})$. The minimization process is implemented using the function `optimize.minimize.fmin` of the library `SciPy`. To obtain an initial guess for the parameters, we use $R_{dry,0} = R_{geom}$ where R_{geom} is the thermal resistance of the given heat pipe based on its geometry, and $K_{loss} = K_{loss,0}$ and $\alpha_{loss} = \alpha_{loss,0}$ being $K_{loss,0} = 0.5$ (in SI units) and $\alpha_{loss,0} = 0.2$.

A comparison of the measured heat applied during the experiments and the heat estimated using Eq. (4) is shown in Fig. 6. The fitting parameters thus obtained are depicted in Table 1. Notice that, since $\alpha_{loss} \approx 1$, we approximate the units of K_{loss} to $\mathrm{W\,K^{-1}}$.

Table 1: Fitting parameters of Equation (4).

R_{dry} [$\mathrm{K\,W^{-1}}$]	K_{loss} [$\mathrm{W\,K^{-1}}$]	α_{loss}
7.48	0.0702	0.9752

The first (Q_{hp}) and second (Q_{loss}) terms of the right-hand side of Eq. (4) are also represented in the same plot. As it can be seen, heat losses are not negligible, and therefore they are calculated using the fitting parameters obtained from dry tests data. Then, these parameters are used to determine the actual heat transfer rate (Q_{hp}) that is used in the calculation of the thermal resistance of the heat pipe filled with acetone. Other authors [11] have also remarked on the need to include heat losses in the transient operation of heat pipes.

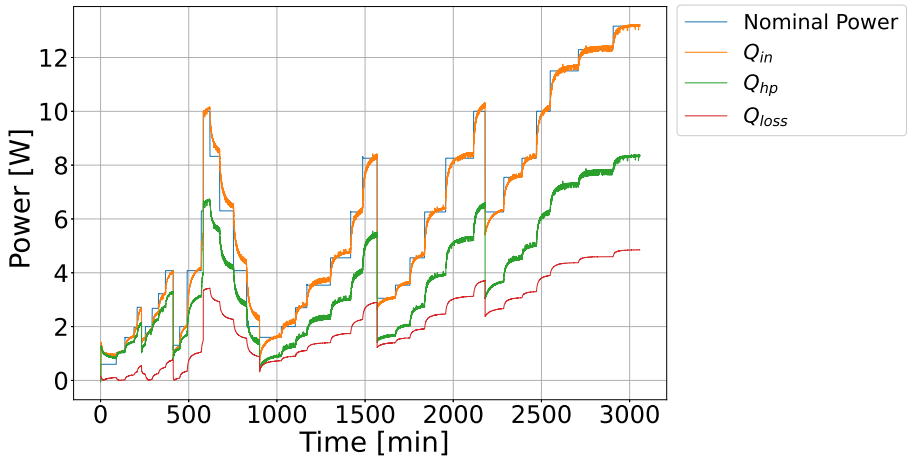

Figure 6: Comparison of the measured heat transfer rate supplied by the heater (Nominal power) and the numerical solution for Q_{in}. Estimate values for Q_{hp} and Q_{loss} are also included.

3. Results and discussion

As an example of our experimental methodology, we describe a series of experiments in which we investigate the effect of the volume of loaded working fluid (the so-called fluid inventory, V) and working mode (thermosyphon or pure heat pipe *i.e.* horizontal) on heat pipe performance. In particular, we consider two performance parameters: the thermal resistance and the response time to a sudden change in the input power. While the first one is customarily used to characterize the performances of heat pipes, to the best of our knowledge, there is no data in the literature of the response time of heat pipes manufactured additively.

Table 2 summarizes the experimental runs performed on the heat pipe prototype. In experiments 1-4 the heat pipe is kept vertical, thus working as

a thermosyphon, during the whole duration of the experiment. Conversely, for experiments 5-7 the heat pipe is started-up vertically with the procedure described in Section 2 and then aligned with the horizontal direction for the test. The fluid inventories used in this work sweep a range around the expected optimal fluid inventory, which is the volume required to fill the wick ($V_w = 0.95\,\mathrm{ml}$).

In this way, we can explore the sensitivity of the heat pipe performances to moderate departures from the optimal inventory. For the thermosyphon configuration, we used four different fluid inventories. After examining the data, it was found that the fluid inventory $V = 3$ ml was significantly greater than the optimal fluid inventory, resulting in high thermal resistance values. As a result, it was not used in the horizontal configuration experiments. To compare with the results obtained from other authors, we include in Table 2 the parameters they use. Chang *et al.* [4] expressed the filling ratio as V/V_t, ratio between the volume of loaded working fluid and the total inner space of the heat pipe (V_t), whereas Jafari *et al.* [8] expressed it as V/V_w (ratio between the volume of loaded working fluid and the volume of the wick). Note that in the current work, some of the loaded fluid V goes to the tube connecting the pipe and to the dead volume of the filling valve, and it is V_{eff} the part of the loaded volume that will fill the heat pipe itself. These ratios were calculated for each experiment and are included in Table 2.

Table 2: Summary of the different experiments reported in this section. In the column "configuration", V stands for vertical (thermosyphon) and H for horizontal (pure heat pipe).

Exp.Number	**Configuration**	V [ml]	V_{eff} [ml]	V_{eff}/V_t	V_{eff}/V_w
1	V	1	0.241	0.039	0.255
2	V	1.5	0.741	0.119	0.783
3	V	2	1.241	0.199	1.312
4	V	3	2.241	0.360	2.369
5	H	1	0.241	0.039	0.255
6	H	1.5	0.741	0.119	0.783
7	H	2	1.241	0.199	1.312

During the experiments, once the heat pipe is started up, the input heat power Q_{in} is varied in steps and the temperatures are measured at different locations as a function of time. The sampling rate of these measurements is high enough to achieve a good time resolution during the transient that occurs after the input power is suddenly changed. The prescribed locations at the outer surface of the heat pipe where the temperatures are measured are: evaporator region bottom and lateral surface (Evp-Bot 1 and Evp-Side-R, respectively); adiabatic section bottom surface (Adb-Bot) and condenser region bottom and lateral surface (Cnd-Bot and Cnd-Side-R, respectively). These measuring points are schematized in Fig. 7(a).

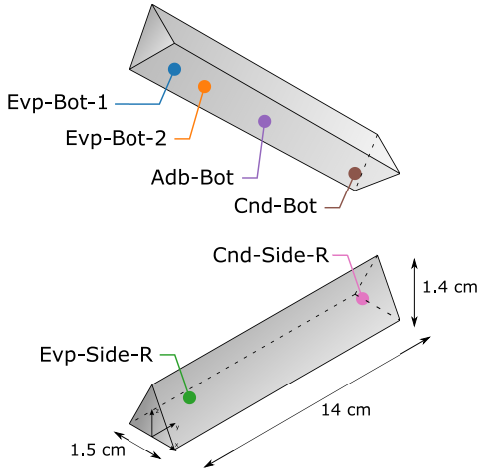

(a)

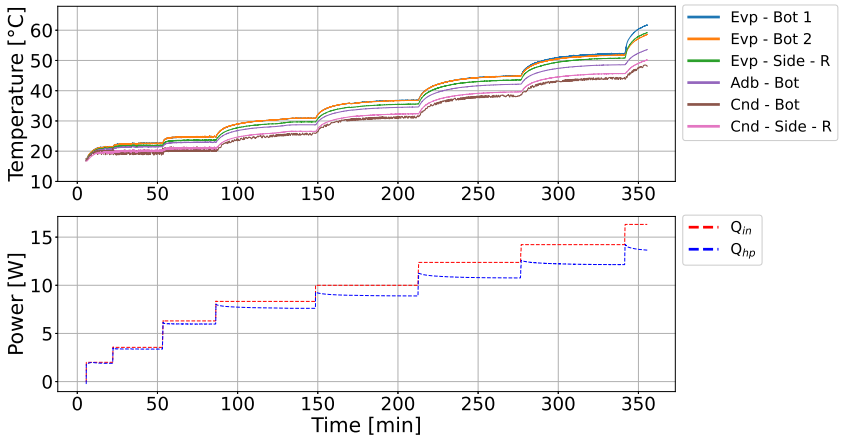

(b)

Figure 7: **(a)** Sketch showing the thermocouples' locations. **(b)** Results of temperature time evolution (up) and input heat transfer rate (down) measured experimentally with $V = 1.5$ ml in horizontal configuration.

The time evolution of the temperatures at the aforementioned positions, for a test with a fluid inventory of $V = 1.5$ ml and the heat pipe placed horizontally, is depicted in Fig. 7(b) (see Supplemental Material for the

remaining functional tests performed in this research).

The lower plot depicts the heat transfer rate supplied at the evaporator, Q_{in}, and the heat transfer rate actually transmitted to the pipe after subtracting heat losses, Q_{hp}.

In Fig. 7(b) we observe that under a heat transfer rate of 4 W, the condenser temperature is maintained at approximately 20 °C. Then, the condenser temperature increases to a maximum value of 50 °C, providing a temperature difference between condenser and evaporator of approximately 7 °C.

3.1. Thermal Resistance

Fig. 8 displays the evolution of the thermal resistance as the effective heat transfer rate increases for various fluid inventories for vertical and horizontal positions. The thermal resistance decreases with increasing filling ratio, as observed by [4] and [8]. Moreover, the thermal resistance decreases as the heat transfer rate increases, since for low heat loads, a thick liquid film remains in the evaporator at all times, reducing heat transfer [12]. However, for the lowest filling ratio (1 ml) the thermal resistance increases monotonically with heat transfer rate from 4 W onwards in both vertical and horizontal orientations. The maximum heat flux that a heat pipe can transport can be defined as the value at which the thermal resistance begins to rise [12]. In this case, this increase is likely due to the wick drying out. On the contrary, for the vertical thermosyphon configuration (Fig. 8(a)) and the fluid inventories of 1.5 ml, 2 ml and 3 ml, wick dry-out is not observed at heat transfer rates lower than 10 W and the thermal resistance still presents a decreasing tendency. Indeed, the fluid inventory of 1.5 ml has the lowest thermal resistance and maintains a constant value when increasing the ef-

fective heat transfer rate without drying out up to a value of 18 W. The fluid inventory of 1.5 ml corresponds roughly to the calculated mass required to fill the wick with liquid and the heat pipe core with vapor. The filling ratio corresponding to 1.5 ml volume is 11.92% with respect to the internal heat pipe volume and 71.2% concerning the total wick volume. This ratio is similar to the one observed by [4] and [8].

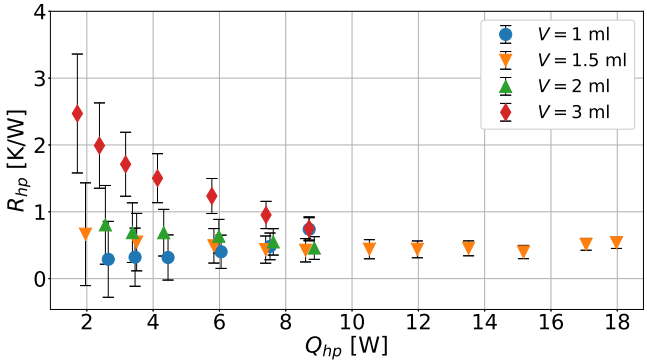

(a) vertical

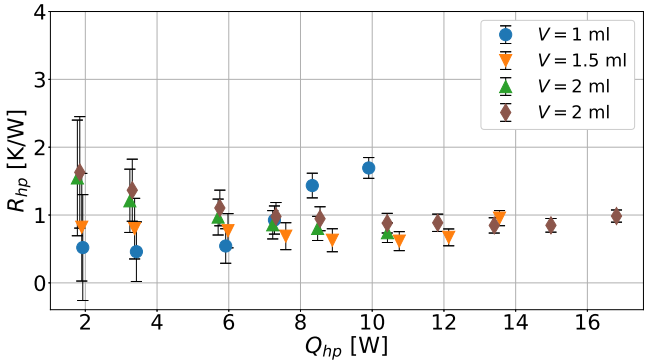

(b) horizontal

Figure 8: Thermal resistance for different fluid inventories (V) as a function of the heat transfer rate in **(a)** vertical and **(b)** horizontal configuration.

Because the horizontal configuration is the most common in industrial applications, the tests were also performed in this orientation (Fig. 8(b)). The fluid inventory of 3 ml was discarded because it was clearly demonstrated to be significantly higher than the optimal inventory. Additionally, the 2 ml test was repeated, and the results of both tests are displayed in Fig. 8(b), demonstrating good repeatability. The 1.5 ml inventory exhibits the lowest thermal resistance, with a value only 25% higher than the resistance measured in the thermosyphon configuration. However, the thermal resistance for this inventory increases for a heat transfer rate larger than 12 W, whereas for an inventory of 2 ml, the thermal resistance remains roughly constant until 17 W, when a slight increase is observed. The thermal resistances shown in Fig. 8 were calculated using Eq. (1), which considers only the heat that is transferred to the prototype Q_{hp}, i.e. the heat supplied by the heater minus heat losses. Thermal resistance values measured for the presented prototype are of the same order of magnitude as those reported by [6] for a comparable applied heat flux.

3.2. Transient Response

Fig. 9 represents the characteristic time of the temperature evolution measured at the evaporator and fitted with the procedure explained in Section 2.3, as a function of the effective heat transfer rate (Q_{hp}). For low values of Q_{hp}, the evaporator heats up almost instantaneously, and an exponential like behavior is not observed, as can be seen for heat fluxes lower than 6 W in the experiment shown in Fig. 7(b). Thus, the characteristic time is not represented in these cases. For larger values of Q_{hp}, the characteristic time is in the range of 500-1500 s as shown in Fig. 9. The results show that the input heat has no significant effect on the characteristic time,

as also reported in the analytical works published by [13]. These analytical models were then compared with the transient temperature profiles measured during the startup and shutdown of a copper flat-plate heat pipe [14]. This research suggested that the convection heat transfer coefficient on the outside water-cooled condenser surface strongly affects the time it takes to reach a steady state, while input power has only a slight effect.

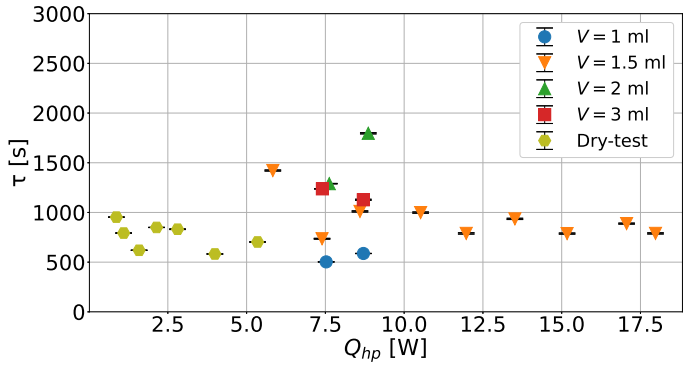

(a) vertical

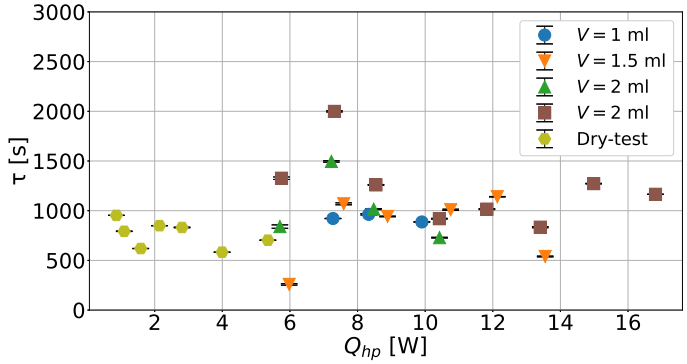

(b) horizontal

Figure 9: Characteristic time of the time evolution temperatures at the evaporator as a function of heat transfer rate for different fluid inventories (V) in **(a)** vertical and **(b)** horizontal configurations.

4. Conclusions

The objective of the current investigation is to propose a novel experimental facility dedicated to the quick and efficient evaluation of heat pipe performances. The experimental procedure includes a methodology to determine the heat losses to the ambient and the steady state temperature from the unsteady measured profiles, which is required for an accurate analysis of the heat pipe characteristics. Moreover, the study seeks to validate experimentally the suitability of the proposed design of an additively manufactured heat pipe to transport heat while upholding a minimal temperature gradient along its entire length.

This research also placed emphasis on examining the influence of controlling the filling ratio, the so-called fluid inventory. Such investigation shows values of the heat pipe thermal resistance, R_{hp}, as low as 0.53 $\mathrm{K\,W^{-1}}$ for a maximum heat transfer rate of 18 W in the vertical thermosyphon configuration. The filling ratio that provides this result is 11.9% with respect to the internal heat pipe volume and 78.3% concerning the total wick volume. The same inventory exhibits the lowest thermal resistance in the horizontal configuration, with a value that is only 25% higher than in the thermosyphon configuration. However, a higher fluid inventory is needed in this orientation to operate the heat pipe up to a heat transfer rate of 17 W without degrading thermal performance. Finally, values of the characteristic time of the time evolution temperature at the evaporator region are presented. These values are not substantially affected, within the experimental uncertainty, by the thermal power that the heat pipe transports, nor by the amount of fluid inventory.

Acknowledgments

The authors acknowledge the financial support of the Regional Government of Madrid through the Industrial Doctorate program, Grant No. IND2019-TIC-17109.

References

[1] J. Jose, T. K. Hotta, A comprehensive review of heat pipe: Its types, incorporation techniques, methods of analysis and applications, Thermal Science and Engineering Progress 42 (2023) 101860.

[2] M. Ando, A. Okamoto, K. Tanaka, M. Maeda, H. Sugita, T. Daimaru, H. Nagai, On-orbit demonstration of oscillating heat pipe with check valves for space application, Applied Thermal Engineering 130 (2018) 552–560.

[3] J. Esarte, J. Blanco, A. Bernardini, R. Sancibrián, Performance assessment of a three-dimensional printed porous media produced by selective laser melting technology for the optimization of loop heat pipe wicks, Applied Sciences 9 (2019) 2905.

[4] C. Chang, Z. Han, X. He, Z. Wang, Y. Ji, 3D printed aluminum flat heat pipes with micro grooves for efficient thermal management of high power LEDs, Scientific Reports 11 (2021) 8255.

[5] Y. Park, I. Bang, Experimental study on 3D printed heat pipes with hybrid screen–groove combined capillary wick structure, Applied Thermal Engineering 232 (2023) 121037.

[6] M. Yun, W.-T. Hsu, D. Shim, J. Nam, J. H. Heo, J.-Y. Song, K. T. Park, D. H. Lee, H. H. Cho, Design and fabrication of heat pipes using additive manufacturing for thermal management, Applied Thermal Engineering 236, Part B (2024) 121561.

[7] C. Buchner, D. Cabelka, J. Gerger, M. Happl, Development of a 3D-

printed heat pipe for thermal management of a high-power CubeSat thruster, in: European Space Thermal Engineering Workshop, 2020.

[8] D. Jafari, W. Wits, B. Geurts, Phase change heat transfer characteristics of an additively manufactured wick for heat pipe applications, Applied Thermal Engineering 168 (2020) 114890.

[9] S. W. Chi, Heat pipe thoery and practice, McGraw Hill, Washington, 1976.

[10] P. Setiani, N. Watanabe, R. Sondari, N. Tsuchiya, Mechanisms and kinetic model of hydrogen production in the hydrothermal treatment of waste aluminum, Materials for Renewable and Sustainable Energy 7 (2018) 10.

[11] A. Kiper, G. Feric, M. Anjum, T. Swanson, Transient analysis of a capillary pumped loop heat pipe, in: 5th Joint Thermophysics and Heat Transfer Conference, Seattle,WA,U.S.A., 1990. doi:https://doi.org/10.2514/6.1990-1685.

[12] R. Hopkins, A. Faghri, D. Khrustalev, Flat miniature heat pipes with micro capillary grooves, Journal of Heat Transfer 121 (1999) 103–109.

[13] Y. Wang, K. Vafai, Transient characterization of plate heat pipes during startup and shutdown operations, International Journal of Heat and Mass Tranfer 43 (2000) 2641–2655.

[14] Y. Wang, K. Vafai, An experimental investigation of the transient characteristics on a flat-plate heat pipe during startup and shutdown operations, ASME Journal of Heat Tranfer 122 (2000) 525–535.